Spin locking and freezing phenomena in the antiferromagnetic Heisenberg model on the three-leg ladder

M. Azzouz* and K. A. Asante
Department of Physics and Astronomy, Laurentian University, Ramsey Lake Road, Sudbury, Ontario, Canada P3E 2C6
(Received 15 April 2005; published 27 September 2005)

The antiferromagnetic Heisenberg model on the three-leg ladder is studied using the generalized Jordan-Wigner transformation in dimensions higher than 1, and the bond-mean-field theory. The magnetic susceptibility and other thermodynamic quantities are analyzed as a function of the rung-to-leg coupling ratio α and temperature T. We fit the experimental susceptibility data of the three-leg material $Sr_2Cu_3O_5$ of Azuma and co-workers with good agreement. One of the main findings of this work is the proposal that close to two-thirds of the spin degrees of freedom on each of the rungs of the ladder lock at low T for small α, then collectively almost 2/3 of the spin degrees of freedom on all the rungs freeze completely at low T for α greater than a threshold value. The approach developed here can be used to study the three-leg ladder for all values of α, and is thus suitable for the description of the crossover regime between the weak- and strong-coupling regimes.

DOI: 10.1103/PhysRevB.72.094433 PACS number(s): 75.10.Jm, 75.10.Pq

I. INTRODUCTION

The Heisenberg ladders have received considerable attention in the past decade or so because some experimental materials have this geometry and because of the search for exotic electronic states in condensed matter.[1–3] The two-leg ladder has been the subject of numerous studies, which have shown that this system has gapped low-energy excitations (see Refs. 2 and 4 and references therein). There has been a conjecture according to which the ladders with an even number of legs have a gapped spectrum, but those with an odd number of legs have a gapless energy spectrum.[5] Johnston *et al.*[6] used the quantum Monte Carlo (QMC) technique to study the three-leg ladder, and found that indeed the low-lying excitations do not show an energy gap. Frischmuth, Amon, and Troyer[7] have also used the QMC technique in a study of ladders with $n_l=1,2,\ldots,6$ legs. Their results confirmed the conjecture concerning the parity of the number of legs. In addition, they found that in the low-energy limit, a one-dimensional (1D) effective Hamiltonian can be defined for $n_l=3$ and 5. This Hamiltonian describes the interaction between the lowest-lying spin doublets in the limit of strong rung-to-chain couplings ratio α. However, they noted that as α decreases $(1/\alpha\rightarrow 1)$, which means that the interaction between the spins along the chains becomes comparable to the interaction along the rungs, the effective Hamiltonian becomes inaccurate, and higher-energy excitations start contributing for temperatures much smaller than in the larger-α limit case. A crossover between the larger-α regime and the lower-α one therefore takes place. We will analyze this crossover in depth in this work. While the strong-coupling regime of the three-leg ladder has been studied using the strong-coupling series expansion,[8] the weak- and intermediate-coupling regimes have been studied using mainly the QMC technique. Note that the bosonization approach has also been used in the weak-coupling regime.[9] This method is, however, not suitable for the intermediate- and strong-coupling regimes. We develop here an approach which can be used to study the crossover between the weak- and strong-coupling regimes.

In this work, we use the bond-mean-field theory[10] (BMFT) and the one of the authors two-dimensional (2D) Jordan-Wigner (JW) transformation of one of the authors[10,11] to study the Heisenberg three-leg ladder. We confirm the QMC results of Johnston *et al.* regarding the existence of a gapless spectrum for all values of α, and show that some of the spin degrees of freedom undergo a partial locking and then freezing depending on T and α. The phenomenon of the locking of some of the spin degrees of freedom takes place for any finite value of α, and is caused by the fact that two of the three spins on a given rung participate in a gapped *state* for any $\alpha>0$, whereas the third remaining spin on this rung forms a doublet, and thus stays available for gapless excitations along the chains. For small α (α smaller than a threshold value α_{tr}), we find that the three-leg ladder geometry becomes irrelevant at high enough temperatures as expected. For $\alpha>\alpha_{tr}$, the three-leg ladder undergoes a geometry crossover below a temperature that is α dependent. Below this temperature, it behaves as a single chain with an effective coupling constant J_{eff} that depends on α, in agreement with the results of Frischmuth *et al.*[7] In this case, not only do some of the spin degrees of freedom lock, but they freeze. The freezing phenomenon can be understood as resulting from the occurrence of the coherence between all the pairs of the spins that are locked on all the rungs. In other words, the freezing phenomenon is obtained when all the spins locked on each rung collectively form a coherent state, where all the pairs of the spins locked into singlets occupy the same two chains (see below for details). We also report features in the magnetic susceptibility that were not seen in existing studies on the three-leg ladder,[12,7] and reanalyze the magnetic properties of the material $Sr_2Cu_3O_5$ that are believed to be modeled by the three-leg ladder structure.[13]

This paper is organized as follows. In Sec. II, we adapt the 2D JW transformation to the three-leg ladder, and review the BMFT used to study this system. This is followed by the derivation of the mean-field equations. The results of this work are presented in Sec. III. These results include the study of the mean-field parameters, the energy spectra, the

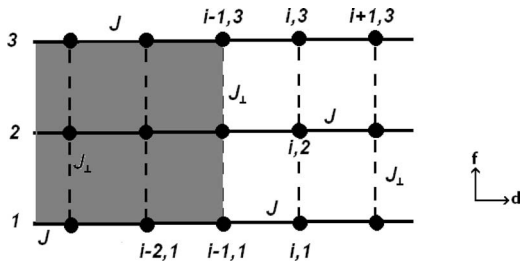

FIG. 1. Sites within the shaded area enter in the summation in the expression of the phase $\Phi_{i,1}$ of $S_{i,1}$ in the JW transformation (2) for the three-leg ladder. The phases for sites $S_{i,2}$ and $S_{i,3}$ are obtained by adding to $\Phi_{i,1}$, $\pi n_{i,1}$, and $\pi(n_{i,1}+n_{i,2})$, respectively.

uniform and static susceptibility and its comparison to existing QMC data, the fitting of the experimental data, and the specific heat analysis. Finally, the conclusions are drawn in Sec. IV.

II. METHOD

A. The Hamiltonian and the JW transformation

The Hamiltonian of the Heisenberg model on the three-leg ladder (Fig. 1) reads as

$$H = \sum_i \left(\sum_{j=1}^{3} J \mathbf{S}_{i,j} \mathbf{S}_{i+1,j} + \sum_{j=1}^{2} J_\perp \mathbf{S}_{i,j} \cdot \mathbf{S}_{i,j+1} \right), \tag{1}$$

where $J>0$ and $J_\perp>0$ are antiferromagnetic (AF) exchange coupling constants along the chains and rungs, respectively, the index $i=0,\ldots,N-1$ labels the N sites on the chains, and the index $j=1,2,3$ labels the chains themselves. We define $\alpha=J_\perp/J$ and set J to be the unit of energies. Assume that we deal with materials where the three chains can be placed on the same plane. Because of the odd number of chains, it is natural to assume open rather than periodic boundary conditions along the rungs. Along the chains the boundary conditions are assumed to be periodic. We plan to report on the case of a triangular nanoprism made of three chains (with periodic boundary conditions) in the future.

The Hamiltonian (1) is transformed using an adapted form of the 2D generalized JW transformation of Ref. 10. Following the notation of Fig. 1, the lowering spin operators at sites $(i,1)$, $(i,2)$, and $(i,3)$, and the z component of the spin operator at site (i,j) are written as follows:

$$S_{i,1}^- = c_{i,1} e^{i\Phi_{i,1}}, \quad \Phi_{i,1} = \pi \sum_{d=0}^{i-1} \sum_{f=1}^{3} n_{d,f},$$

$$S_{i,2}^- = c_{i,2} e^{i\Phi_{i,2}}, \quad \Phi_{i,2} = \Phi_{i,1} + \pi n_{i,1},$$

$$S_{i,3}^- = c_{i,3} e^{i\Phi_{i,3}}, \quad \Phi_{i,3} = \Phi_{i,2} + \pi n_{i,2},$$

$$S_{i,j}^z = n_{i,j} - \frac{1}{2}, \tag{2}$$

where $n_{i,j}=c_{i,j}^\dagger c_{i,j}$ is the occupation operator of the JW spinless fermions. Using (2), the Hamiltonian (1) becomes

$$H = \sum_i \sum_{j=1}^{3} \frac{J}{2} e^{i(\Phi_{i,j}-\Phi_{i+1,j})} c_{i+1,j}^\dagger c_{i,j} + \sum_i \sum_{j=1}^{2} \frac{J_\perp}{2} e^{i(\Phi_{i,j}-\Phi_{i,j+1})} \times c_{i,j+1}^\dagger c_{i,j} + (\text{H.c.}) + J \sum_i \sum_{j=1}^{3} \left(n_{i,j} - \frac{1}{2}\right)\left(n_{i+1,j} - \frac{1}{2}\right) + J_\perp \sum_i \sum_{j=1}^{2} \left(n_{i,j} - \frac{1}{2}\right)\left(n_{i,j+1} - \frac{1}{2}\right), \tag{3}$$

which describes a system of interacting spinless fermions coupled to a gauge field. An analysis of this gauge field and the mean-field treatment analogous to the ones made in Ref. 14 for the Heisenberg bilayer can be made here. Next, we explain how we obtain the mean-field Hamiltonian.

B. The mean-field Hamiltonian

The BMFT consists, first, of approximating the phase differences resulting from the hopping of the JW fermions around any given elementary plaquette by π.[10,14,15] Along the chains, the phases consist for example of the configuration $\ldots 0\text{-}\pi\text{-}0\text{-}\pi\text{-}0\text{-}\pi\ldots$ on the bonds $\ldots(i-1,i)(i,i+1)(i+1,i+2)\ldots$ on the chains 1 and 3, but $\ldots\pi\text{-}0\text{-}\pi\text{-}0\text{-}\pi\text{-}0\ldots$ on the bonds $\ldots(i-1,i)(i,i+1)(i+1,i+2)\ldots$ on chain 2. The phases on all the bonds along the rungs are zero. Second, the quartic Ising terms of the Hamiltonian (1), $\Sigma_{i,j}(n_{i,j}n_{i+1,j}+n_{i,j}n_{i,j+1})$, resulting from the Ising interactions, are decoupled using the bond parameters $Q=|\langle c_{2i,j}c_{2i+1,j}^\dagger\rangle|$ for chain 1 ($j=1$) and chain 3 ($j=3$), and $Q'=|\langle c_{2i,2}c_{2i+1,2}^\dagger\rangle|$ for chain 2 in the direction parallel to the chains. Along the rungs, $P=|\langle c_{2i,j}c_{2i,j+1}^\dagger\rangle|$. This choice is consistent with the fact that the three-leg ladder is symmetric with respect to exchanging the chain labels 1 and 3, but is an example of a system where the order parameter takes on different values depending on whether an internal or external part of the system is considered. Note that this approximation satisfies the Mermin-Wagner theorem since the long-range AF order is not taken into account.[16] So $\langle S_{i,j}^z\rangle=0$ gives $\langle c_{i,j}^\dagger c_{i,j}\rangle=1/2$. The latter implies that the three-leg ladder is half filled with the JW fermions. More details on the BMFT can be found elsewhere.[17,18] Fourier transforming and using the Nambu formalism[19] yield the mean-field Hamiltonian in the form

$$H = \sum_k \Psi_k^\dagger \mathcal{H} \Psi_k + 2NJQ^2 + NJQ'^2 + 2NJ_\perp P^2, \tag{4}$$

where the Nambu spinor is given by

$$\Psi_k^\dagger = (c_{1k}^{A\dagger}\ c_{1k}^{B\dagger}\ c_{2k}^{A\dagger}\ c_{2k}^{B\dagger}\ c_{3k}^{A\dagger}\ c_{3k}^{B\dagger}). \tag{5}$$

Here c_{jk}^a is the Fourier transform of c_{ij}^a in the i index along the chains ($a=A,B$). The Fourier transform is performed in the chains direction only, but not in the rung direction because of the open boundary conditions. The Hamiltonian density is given by

$$\mathcal{H} = \begin{pmatrix} 0 & e(k) & 0 & \frac{J_{\perp 1}}{2} & 0 & 0 \\ e^*(k) & 0 & \frac{J_{\perp 1}}{2} & 0 & 0 & 0 \\ 0 & \frac{J_{\perp 1}}{2} & 0 & e'(k) & 0 & \frac{J_{\perp 1}}{2} \\ \frac{J_{\perp 1}}{2} & 0 & e'^*(k) & 0 & \frac{J_{\perp 1}}{2} & 0 \\ 0 & 0 & 0 & \frac{J_{\perp 1}}{2} & 0 & e(k) \\ 0 & 0 & \frac{J_{\perp 1}}{2} & 0 & e^*(k) & 0 \end{pmatrix}, \quad (6)$$

with $e(k)=iJ_1 \sin k$ and $e'(k)=iJ_1' \sin k$. Notice that because of the AF correlations, the three-leg-ladder lattice is subdivided into two sublattices A and B. Diagonalizing $\mathcal{H}$ yields the energy eigenvalues $\pm E_1(k)$, $\pm E_2(k)$, and $\pm E_3(k)$, where

$$E_1(k) = J_1 \sin k,$$

$$E_2(k) = \frac{1}{2}(J_1 - J_1')\sin k + \frac{1}{2}\epsilon(k),$$

$$E_3(k) = -\frac{1}{2}(J_1 - J_1')\sin k + \frac{1}{2}\epsilon(k), \quad (7)$$

with

$$J_1 = J(1+2Q),$$

$$J_1' = J(1+2Q'),$$

$$J_{\perp 1} = J_\perp(1+2P),$$

$$\epsilon(k) = \sqrt{(J_1 + J_1')^2 \sin^2 k + 2J_{\perp 1}^2}. \quad (8)$$

The excitation energy spectra are obtained by noting that the elementary excitations in the present approach, which is based on the JW fermions, consist of particle-hole excitations.[17] Thus the excitation energies are obtained by subtracting the lower-energy bands from the upper-energy ones and dividing by 2; this gives $|E_j(k)|$ with $j=1,2,3$. The energy spectrum $|E_1(k)|$ has the same form as the des Cloizeaux–Pearson spectrum of the AF Heisenberg chain.[20] $E_2(k)$ and $E_3(k)$ present a form with a gap of the order of $J_\perp$. The excitations energies consist thus of three bands, two of which are gapped. These type of spectra are at the origin of the interesting phenomena of locking and freezing of about two-thirds of the spin degrees of freedom. These phenomena will be studied in detail throughout the remainder of this paper. Next, we start by deriving the mean-field equations.

C. Mean-field equations

In the present mean-field approach, the free energy per site or spin corresponding to Hamiltonian (4) is

$$f = \frac{1}{3}(2JQ^2 + JQ'^2 + 2J_\perp P^2) - \frac{k_B T}{2N_t}\sum_k \sum_{p=\pm} \sum_{j=1}^{3} \ln(1 + e^{p\beta E_j(k)}), \quad (9)$$

where $N_t=3N$ is the total number of lattice sites, and $\beta = 1/k_B T$. The summation over k runs over the reduce 1D Brillouin zone. The parameters Q, Q' and P are determined by minimizing f; i.e., $\partial f/\partial Q = \partial f/\partial Q' = \partial f/\partial P = 0$. This gives

$$Q = \frac{1}{8N}\sum_k \sum_{j=1}^{3} g_j(k)\tanh[\beta E_j(k)/2],$$

$$Q' = \frac{1}{4N}\sum_k \sum_{j=2}^{3} g_j'(k)\tanh[\beta E_j(k)/2],$$

$$P = \frac{1}{8N}\sum_k \sum_{j=2}^{3} g_{j\perp}(k)\tanh[\beta E_j(k)/2], \quad (10)$$

with the dimensionless functions

$$g_1(k) = 2 \sin k,$$

$$g_2(k) = \sin k + (J_1 + J_1')\sin^2 k/\epsilon(k),$$

$$g_3(k) = \sin k - (J_1 + J_1')\sin^2 k/\epsilon(k),$$

$$g_2'(k) = -g_3(k), \quad g_3'(k) = -g_2(k),$$

$$g_{2\perp}(k) = -g_{3\perp}(k) = 2J_\perp(1+2P)/\epsilon(k). \quad (11)$$

III. RESULTS

In this section, we present the numerically calculated solutions of the mean-field equations (10). We begin by analyzing the α and T dependence of the mean-field parameters Q, Q', and P, then we analyze the energy spectra, the uniform and static susceptibility $\chi(T)$, and finally the thermodynamic functions $S(T)$ and $C(T)$.

A. Mean-field parameters

1. α dependence

The α dependence of the mean-field parameters Q, Q' and P at zero temperature is displayed in Fig. 2. For $\alpha \to 0$, $Q' \to Q$ with both approaching the zero-α value, namely, 0.317.[10] The most important feature in Fig. 2 is the difference shown by Q and Q'. This gives rise to an interesting physical situation where the same physical parameter takes on different values depending on the part of the system considered. Q and Q' define the same physical quantity that is the nearest-neighbor bond along the chains; Q is defined on the outer chains, and Q' on the inner chain. Because of the geometry of the three-leg ladder (space anisotropy) the bond parameter P along the rungs behaves differently than Q and Q'. P vanishes at $\alpha=0$. With increasing α, P increases, then

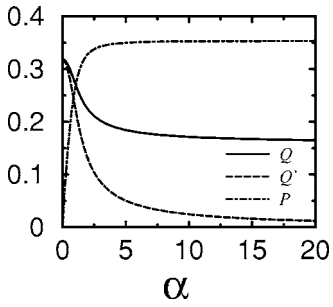

FIG. 2. The mean-field parameters Q, Q', and P are plotted as functions of $\alpha=J_\perp/J$ at zero temperature.

saturates at about 0.35, but Q and Q' decrease, with Q' decreasing faster than Q, and becoming vanishingly small when α is much greater than 1. Q, however, saturates at approximately 0.16. This indicates the formation of strong bonds in the outer chains 1 and 3, and loose bounds in the inner chain 2. The Ising interaction in the inner chain becomes completely irrelevant in the large-α limit as $Q'=0$ in the $\alpha=\infty$ limit means that the spin interactions in the inner chain acquire a purely XY character (remember that Q and Q' result from the decoupling of the Ising terms along the chains).

2. T dependence

From a qualitative point of view, because of strong thermal fluctuations for temperatures much greater than $J_\perp$, all the spins are expected to behave as decoupled along the rungs (as well as along the chains if $T>J$ as a matter of fact), and one expects to recover the case of three loosely coupled chains if $\alpha \ll 1$. This means that Q, Q', and P should decrease as T increases, and $Q-Q'$ should approach zero as temperature increases.

Plots of the mean-field parameters as a function of temperature for different values of α are displayed in Fig. 3. For a given α, the parameters Q, Q', and P have a maximum value at $T=0$. With increasing temperature, they all decrease but do not vanish at any finite temperature, excluding in this way the possibility of a finite-temperature phase transition. Note that in the isotropic case with $\alpha=1$, $Q\approx Q'$ and they differ only slightly from P at low temperature. Also, Q, Q',

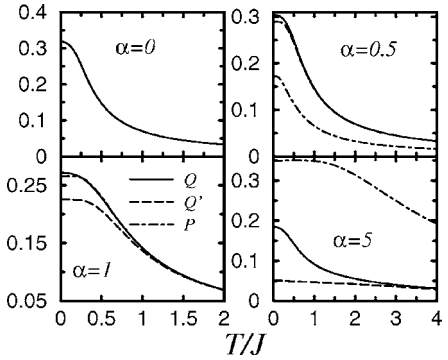

FIG. 3. The parameters Q, Q', and P are plotted as a function of temperature (T/J) for four values of α. For $\alpha=0$, $P=0$ and $Q=Q'$ at any temperatures.

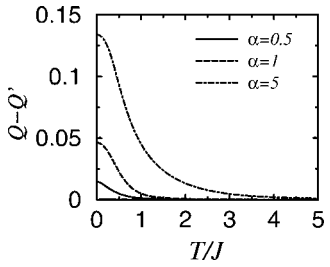

FIG. 4. The quantity $Q-Q'$ is plotted as a function of temperature for three values of α. $Q-Q'$ becomes significantly greater than zero at low temperature.

and P are practically equal for $T>J$. In Fig. 4, we plot the quantity $Q-Q'$ as a function of temperature for three values of α. It is found that $Q-Q'$ decreases significantly as temperature increases, without vanishing sharply at a critical temperature. This also excludes the possibility of a phase transition in the three-leg ladder; therefore one can only talk about a crossover taking place from a high-temperature regime with $Q-Q'\approx 0$ and a low-temperature regime with $Q-Q'>0$.

B. Energy spectra

1. α dependence

In the 1D limit with $\alpha=0$, the excitation spectrum is known exactly, and is given by the des Cloizeaux and Pearson formula[20]

$$\epsilon(k)=\frac{\pi}{2}J|\sin k| \approx 1.57J|\sin k|. \tag{12}$$

In this limit, Eqs. (7) yield $\pm E_1=\pm E_2=\pm E_3=\pm J_1 \sin k$, with $J_1\approx 1.64J$ at $T=0$,[10] which in turn gives the excitation spectrum $1.64J|\sin k|$ in good agreement with the des Cloizeaux–Pearson result (12).

In Fig. 5, we display the energy eigenvalues as a function of the wave vector k for two values of α ($\alpha=1,3$). $E_1(k)$ vanishes at $k=0$ and π, and has a maximum occurring at a lower energy in comparison to the maxima of $E_2(k)$ and $E_3(k)$. E_2 and E_3 show an identical energy gap in the vicinity of $k=0$ or π, but differ around $k=\pi/2$. In the ground state (GS) (i.e., at $T=0$), the energies $E_1(k)$ with $k\sim 0$ and π predominantly contribute to any physical quantity. Because of the gap in E_2 and E_3, their contributions become significant only at high enough temperatures. This is at the origin of the mechanisms of the phenomena of locking for small α's and freezing for larger α's. The energies $E_2(k)$ and $E_3(k)$ contribute significantly to any physical quantity only when the thermal energy is higher than the gap in E_2 and E_3. Figure 6 shows the energy gap in E_2 or E_3 as a function of α. This gap is nonzero for all values of α, and except for small values of α (<0.5, where a slight upward curvature is observed), this gap increases linearly with α.

2. The spin degrees of freedom locking and freezing

The energy spectra for $\alpha=3$ in Fig. 5(b) show that for temperatures smaller than $\sim J$, the lowest band $|E_1|$ practi-

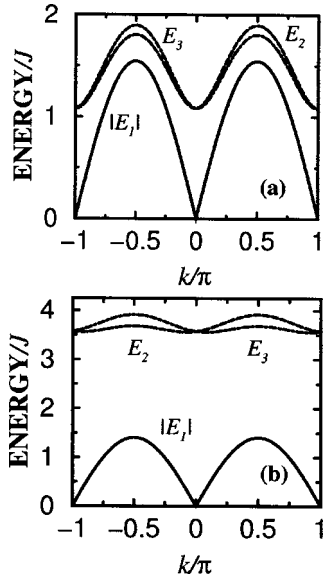

FIG. 5. The excitation spectra $|E_j(k)|$, with $j=1,2,3$, are plotted as a function of k for $\alpha=1$ in (a) and 3 in (b).

cally dominates. The three-leg ladder in this case can be mapped onto a single Heisenberg chain. Indeed, for $\alpha \gg 1$, two of the spins on adjacent sites on any given rung lock into a "singlet" (as we mentioned earlier), leaving the remaining spin on that rung to participate in the formation of a spin-1/2 chain with the effective coupling J_{eff}, given by

$$J_{eff}(\alpha) = JJ_1(\alpha)/J_1(\alpha=0) \quad (\alpha \gg 1), \tag{13}$$

in the low-T limit ($T \ll J_\perp$). Equation (13) is obtained by noting that the actual coupling constant in the linear chain is obtained by dividing the coefficient $J\pi/2$ of the des Cloizeaux–Pearson spectrum by $\pi/2$ for the single chain or by $J[1+2Q(\alpha=0)]=J_1(\alpha=0)$ in the BMFT for the three-leg ladder. This generates a renormalization of the coupling along the chains by the coupling along the rungs. Thus, for nonzero α, the three-leg ladder behaves as a combination of a spin-1/2 chain and a two-leg ladder for $T \ll \alpha J = J_\perp$. The energy spectra (7) are in agreement with this assessment. $E_1(k)$ is a renormalized des Cloizeaux–Pearson spectrum, and can be viewed as the energy spectrum of one of the outer chains, and $E_2(k)$ and $E_3(k)$ as the energy spectra of the remaining two chains. Note that for the chain with $E_1(k)$, the spin velocity $J[1+2Q(\alpha)]$ is renormalized by the α dependence of Q, Fig. 2. The effective interaction J_{eff} for this chain is also renormalized with respect to the single Heisenberg chain; Eq. (13) shows that J_{eff} reduces to J as expected when $\alpha=0$, but as seen in Fig. 7, J_{eff} is reduced by about 18% with respect to J in the large-α limit.

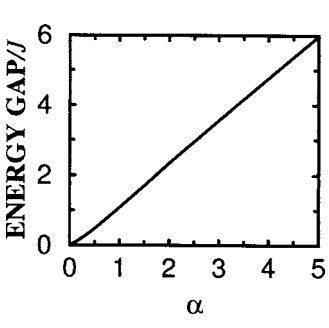

FIG. 6. The energy gap in E_2 or E_3 is drawn versus α.

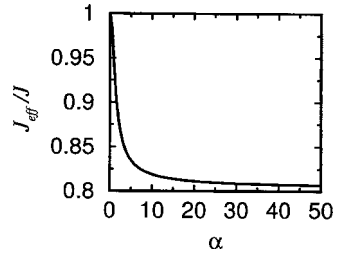

FIG. 7. The effective coupling constant J_{eff} is plotted as a function of α.

Based on the energy spectra in Fig. 5, at zero temperature the band E_1 contributes the most, which gives a 1D spin system with the coupling J_{eff} even if $J_\perp$ is finite. In fact, the chain with the effective coupling J_{eff} is an excellent approximation for the three-leg ladder in the large-α limit, in agreement with the results of Frischmuth *et al.*[7] and Reigrotzki *et al.*[21] Note that for small $\alpha < 1$, $J_{eff} \approx J$ is also in agreement with the work of these authors.

C. The uniform and static susceptibility

1. The magnetization along the z-axis

In the present approach, the rotational symmetry is not broken because of the absence of long-range AF order. The mean-field approximation nonetheless breaks the spin space isotropy as a consequence of fixing the quantization axis in the JW transformation. Consequently, the spin response is anisotropic. For convenience reasons, we will calculate the spin susceptibility in the z direction; the susceptibility in the xy plane being much more difficult to calculate, we will use an estimate from the work of Muthukumar *et al.*[22] In terms of the JW fermions, a magnetic field H applied along the spin z axis becomes a chemical potential for the JW fermions; the energy term corresponding to it is $-h\Sigma_i\Sigma_{j=1}^3 S_{i,j}^z = -h\Sigma_i\Sigma_{j=1}^3 (c_{i,j}^\dagger c_{i,j} - 1/2)$, with $h=g\mu_B H$. Here, g is the Landé factor, and μ_B the Bohr magneton. For the purpose of calculating the magnetization, the energy spectra can be approximated by $\pm E_j(k) - h$ ($j=1,2,3$) in the limit of a very weak magnetic field. The magnetization, normalized with respect to $g^2\mu_B^2$, is found by calculating the free energy per site $f(h,T)$, then differentiating with respect to h: $M_z(h,T) = -\partial f(h,T)/\partial h$. In the limit of a very weak magnetic field ($h \sim 0$), one obtains for the magnetization

$$M_z(T,h) \approx \frac{1}{N_t} \sum_{k,p=\pm} \sum_{j=1}^{3} n_F[pE_j(k) - h] - \frac{1}{2}, \tag{14}$$

where $n_F(x)=(1+e^{\beta x})^{-1}$ is the Fermi-Dirac factor. So the magnetization turns out to be the average number of the JW fermions per site minus 1/2. In the absence of an external magnetic field the lattice is half filled, leading to $M_z=0$.

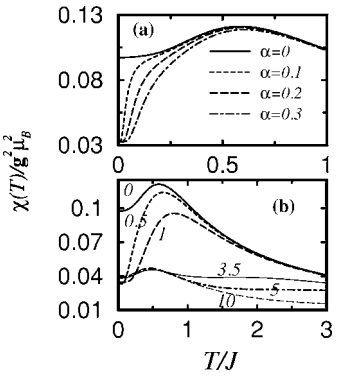

FIG. 8. The susceptibility is drawn versus temperature for various values of α: (a) $0<\alpha<0.4$, (b) $0<\alpha<10$.

Experimentally, a spatially averaged spin susceptibility is measured for polycrystalline materials. Following Muthukumar and co-workers,[22] one finds $\chi(T)=[\chi_{xx}(T)+\chi_{yy}(T)+\chi_{zz}(T)]/3\approx\chi_{zz}(T)/2$. The uniform and static susceptibility $\chi(T)$ can therefore be obtained by applying a static and uniform magnetic field H parallel to the z axis. The zero-field susceptibility in the z direction is $\chi_{zz}(T)=\partial M/\partial h|_{h=0}=-\partial^2 f/\partial h^2|_{h=0}$, which leads to the following result for the susceptibility per spin:

$$\chi(T)=\frac{8\beta}{3}\sum_{j=1}^{3}\int\frac{dk}{2\pi}\cosh^{-2}\left(\frac{\beta E_j(k)}{2}\right). \tag{15}$$

The factor 1/3 in Eq. (15) is a consequence of dividing by the total number of sites $3N$.

2. Zero-temperature value of $\chi(T)$

For $J_\perp\gg T$, only the term of $\chi(T)$ in which E_1 is involved dominates because E_2 and E_3 are gapped. So the zero temperature value of $\chi(T)$ can be expected to be roughly the third of what it is for a single Heisenberg chain; i.e., when $\alpha=0$. For $J_\perp\gg T$ with $T\to 0$, $\chi(T)$ is approximately given by the density of state of the JW fermions at the Fermi level $\epsilon_F=0$:

$$\chi(T=0,\alpha)\approx\frac{1}{3}\chi(T=0,\alpha=0)=\frac{1}{3\pi v_s}, \tag{16}$$

where $v_s=(1+2Q)J$ is the spin velocity of the spin excitations along a single AF chain. Equation (16) is indeed in good agreement with our numerical calculation, the results of which are presented in Fig. 8(a). $\chi(T)$ is displayed versus temperature for several values of α. We clearly see that $\chi(T=0,0<\alpha<1)\approx 0.032$ whereas $\chi(T=0,\alpha=0)\approx 0.097$, which is three times greater.

3. Nonzero-temperature susceptibility

From a qualitative point of view, in the high-temperature regime with $T\gg J_\perp$, one expects no significant difference between $\chi(T,\alpha>0)$ and $\chi(T,\alpha=0)$. In this regime, thermal fluctuations unlock the spin singlets because they overcome the effect of $J_\perp$ (or the gap due to $J_\perp$). This is found to be the case indeed, but for only $\alpha<\alpha_{tr}$, as seen in Fig. 8, with $\alpha_{tr}\approx 2.75$. Figures 8(a) and 8(b) show $\chi(T)$ versus temperature for several values of α between 0 and 10. For small α in panel (a), $\chi(T)$ rapidly increases with temperature and reaches the 1D susceptibility at a temperature that increases with $J_\perp$. This demonstrates that as temperature increases the three-leg ladder geometry becomes irrelevant; the three-leg ladder behaves as if it were 1D at high enough T. For $\alpha<\alpha_{tr}$, $\chi(T)$ shows a single maximum that decreases when α increases.

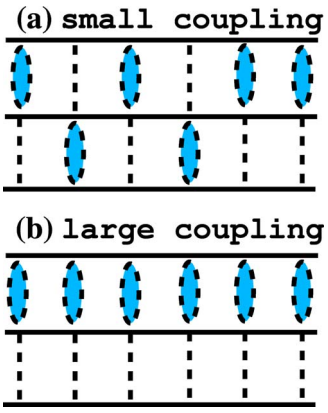

FIG. 9. (Color online) Low-T schematic representation of spin locking (a) and freezing (b). (a) $\alpha<\alpha_{th}$: there is no preferred location for the "singlets;" each "singlet" can jump back and forth between the two top and two bottom chains. We say that the singlets form a fluid state. (b) $\alpha>\alpha_{th}$: the "singlets" occupy either the two top (like here) or the two bottom chains; the three-leg ladder in this case behaves as a combination of a single chain and a two-leg ladder. A dashed ellipse symbolizes a pair of spins locked into a singlet.

At α_{tr}, the maximum of $\chi(T)$ splits into two maxima which are smaller than the original maximum. This signals a regime change, in which the spin degree of freedom freeze for temperatures well below $J_\perp$. The freezing phenomenon can now be understood by the fact that the spin singlets on each rung order coherently along two of the three chains as illustrated in Fig. 9. The maximum in $\chi(T)$ at the lower temperature has the same origin as the maximum in the susceptibility of a single Heisenberg chain; i.e., the quantum fluctuations (at low T) become important enough to level off the increase of the susceptibility as T decreases to zero. However, the maximum at the higher temperature is due to the fact that as T increases the spin degrees of freedom frozen in the singlets "defrost," thus causing the susceptibility to increase before it is brought down by the thermal fluctuations at higher temperatures. Figure 10 illustrates the region of α where the regime change takes place. For $\alpha<\alpha_{tr}$, $\chi(T)$ has a single maximum. For $\alpha>\alpha_{tr}$, this maximum splits into two maxima as seen for $\alpha=3$. Note that the higher-T maximum becomes less pronounced for larger values of α as it occurs in a region of temperature which is dominated by the classical thermal fluctuations.

The regime change taking place at α_{tr} can be best seen by focusing on the temperature T_{max} at which the maximum (the first of the maxima when $\alpha>\alpha_{tr}$) of $\chi(T_{max})$ occurs. In Fig.

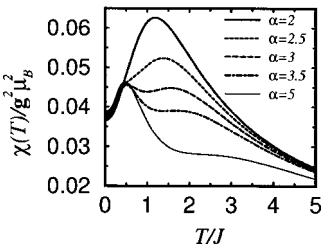

FIG. 10. The susceptibility is drawn versus temperature for values of α near the threshold value $\alpha_{tr} \approx 2.75$.

11, T_{max} is displayed as a function α. T_{max} increases with $\alpha < \alpha_{tr}$, then at α_{tr}, it drops back close to the 1D ($\alpha=0$) value. Above α_{tr}, the contribution of the band E_1 is much greater than that of the bands E_2 and E_3 in the low-temperature regime, ($T \ll J_\perp$). Indeed, Fig. 12 shows that the susceptibility is predominantly given by the contribution from the band E_1, that is,

$$\chi_{eff} = \frac{8\beta}{3} \int \frac{dk}{2\pi} \cosh^{-2}[\beta E_1(k)/2]$$

for $T \ll J_\perp$. In the strong-coupling region $\alpha > \alpha_{tr}$, T_{max} assumes precisely the value $T_{max} = T_{max}(\alpha=0) \times J_{eff}/J \approx 0.46J$, which agrees very well with the numerical value in Fig. 11. This is smaller than the 1D value of $T_{max} = 0.58J$.

D. Interpretation of locking and freezing of the spin degrees of freedom

In summary, below the threshold value α_{tr}, the coupling along the rungs $J_\perp$ causes the locking of part of the spin degrees of freedom at very low temperatures. Above α_{tr}, the spin degrees of freedom freeze for temperature well below $J_\perp$; for $\alpha=10$, Fig. 12 shows that the three-leg ladder undergoes a dimensionality crossover, as far as the magnetic degrees of freedom are concerned, from the three-leg geometry to strict one-dimensionality at a temperature of about $2J$.

To understand this behavior, consider the limit $\alpha=\infty$ with $J=0$ and $J_\perp=1$. The states of the system in this case are the GS doublet with $-J_\perp$ and spin 1/2, a doublet with energy zero and spin 1/2, and a quartet with energy $J_\perp/2$ and spin 3/2. Switching on a small coupling J along the chains effectively couples the GS doublets, and thus yields a system equivalent to a Heisenberg chain with the effective coupling

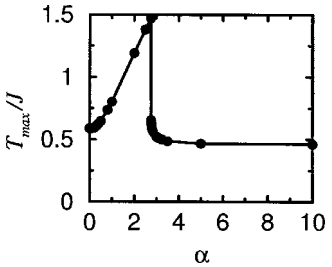

FIG. 11. The temperature T_{max}, at which the maximum (the first of the maxima for $\alpha > \alpha_{tr}$) of $\chi(T)$ takes place, is plotted as a function of α.

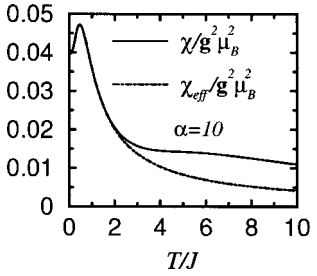

FIG. 12. The susceptibility $\chi(T)$ is drawn versus temperature for $\alpha=10$. It is compared with the contribution χ_{eff} from the E_1 term in Eq. (15). For $T<2J$, χ_{eff} coincides exactly with the total susceptibility $\chi(T)$.

J_{eff}, which is renormalized by $J_\perp$. To involve the spin degrees of freedom in the state above the GS doublet one needs to overcome an energy separation of the order of $J_\perp$.[21] When $J_\perp \gg J$, the mapping of the three-leg ladder onto a single Heisenberg chain becomes practically exact even for $T<J$. For $J_\perp < J$ (precisely for $J_\perp < 2.75J$ as we find here), however, this mapping breaks down.

Later on, we will examine the specific heat and study how the freezing phenomenon of the spin degrees of freedom is reflected in it. But first, we compare our susceptibility results to the QMC results,[6] and attempt to fit the experimental data of the material $Sr_2Cu_3O_5$,[13] which is believed to be a three-leg ladder as far as the magnetic properties are concerned.

E. Comparison with the quantum Monte Carlo results

Using the QMC technique, Johnston *et al.*[6] calculated the spin susceptibility as a function of temperature for several values of α with $0 \leqslant \alpha \leqslant 1$. Although our numerical values of χ do not agree well with those these authors obtained, because our susceptibility is off by about 20%, the trends in $\chi(T)$ as a function of α we get agree very well with theirs. The sudden decrease of $\chi(T=0)$ as α becomes nonzero was also observed in the QMC results, and provides a strong evidence for the qualitative applicability of the BMFT in the case of the three-leg ladder. The difference $\chi(T=0,\alpha=0) - \chi(T=0, 0<\alpha \ll 1) \approx 0.063$ we calculated is in good agreement with their result 0.070.

F. Fitting the experimental susceptibility data of $Sr_2Cu_3O_5$

We now fit the experimental susceptibility data of Azuma *et al.*[13] for the three-leg ladder material $Sr_2Cu_3O_5$. Following the approach of Johnston *et al.*,[6] we make a fit using the expression

$$\tilde{\chi}(T) = N_A \frac{g^2 \mu_B^2}{J} \chi(T), \tag{17}$$

where $N_A = 6.022 \times 10^{23}$ mol^{-1} is Avogadro's number. Using $g=2$ Eq. (17) can be written in the cgs unit system as

$$\tilde{\chi}(T) \approx 1.5(\text{cm}^3\ \text{K mol}^{-1}) \frac{1}{J/k_B} \chi(T). \tag{18}$$

The values of the coupling constants used to fit the data are $J/k_B = 1700$ K and $\alpha=0.4$. The result is reported in Fig. 13.

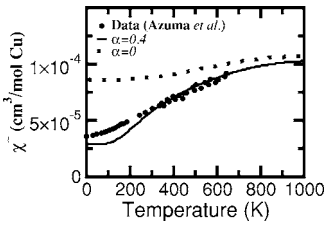

FIG. 13. The experimental magnetic susceptibility of $Sr_2Cu_3O_5$ from Ref. 13 is shown as circles. The solid line is our theoretical fit obtained using the coupling constants $J/k_B=1700$ K and $\alpha=J_\perp/J=0.4$. For comparison the dotted line is the susceptibility calculated for the one-dimensional ($J_\perp/J=0$) case with $J/k_B=1700$ K.

The range of temperature of the experimental data of Azuma *et al.*[13] is from 5 to 650 K. From our fit in Fig. 13, we observe good agreement with the experimental data above about 320 K. However, in the lower-temperature region deviations from the experimental data exist. We believe that the departure of our theoretical curve from the experimental data can be attributed to the fact that the BMFT does not account for all the spin correlations. For comparison we also show in Fig. 13 the susceptibility of the linear chain we calculated for $\alpha=0$ within the BMFT. This is displayed as a dotted line. This shows that a finite value of α is needed to obtain an acceptable fit of the experimental data, and rules out the possibility that the magnetic properties of $Sr_2Cu_3O_5$ are described by a linear Heisenberg chain. The maximum of $\chi(T)$ for this material would occur at $T_{max}\approx 0.58\times 1700=986$ K. Note that the temperature at which this compound starts to decompose is about 800 K.[23]

G. Specific heat analysis

1. Entropy

The entropy per spin, $S=-\partial f/\partial T$, is given by

$$S=\frac{-k_B}{2N_t}\sum_{k,p=\pm}\sum_{j=1}^{3}(n_F[pE_j(k)]\ln n_F[pE_j(k)] + \{1-n_F[pE_j(k)]\}\ln\{1-n_F[pE_j(k)]\}), \quad (19)$$

where $E_j(k)$ represents the eigenenergies defined in Eq. (7). Plots of the entropy, normalized by the Boltzmann constant, are displayed in Fig. 14(a) for various values of α. Again, for small α, one notices, as for the spin susceptibility, that the density of states is reduced by a factor of roughly 3 when α becomes nonzero, because of the spin-locking phenomenon. This is seen as the reduction of the slope of $S(T)$ in the vicinity of zero T for nonzero α.

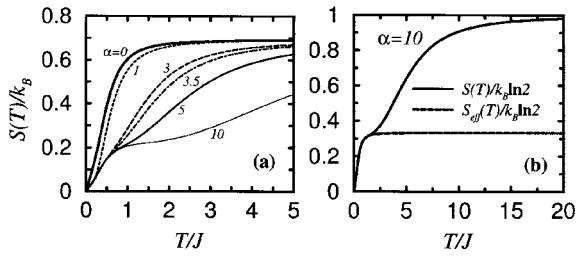

FIG. 14. (a) The entropy is displayed as a function of temperature for several values of α. (b) The entropy for $\alpha=10$ is compared to the entropy contribution of the lower-energy band E_1. Both entropies are equal for $T<2J$.

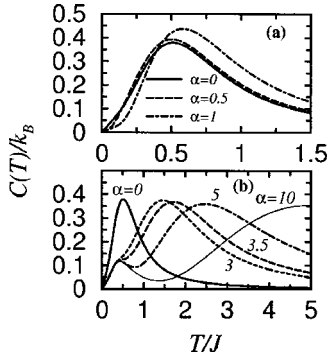

FIG. 15. The specific heat is drawn as a function of T: (a) for $0\leqslant\alpha\leqslant 1$, (b) for greater values of α together with the $\alpha=0$ curve.

In Fig. 14(b), the entropy divided by $k_B\ln 2$ is displayed as a function of T for $\alpha=10$. $S(T)/k_B\ln 2$ clearly presents two regimes; in the first regime realized for $T<2J$, the entropy accounts for only the third of the spin degrees of freedom, as given by

$$S_{eff}=-\frac{k_B}{2N_t}\sum_{k,p=\pm}\{f(pE_1)\ln f(pE_1) + [1-f(pE_1)]\ln[1-f(pE_1)]\}, \quad (20)$$

which is the contribution from the $E_1(k)$ band only. In the second regime, the entropy is rather a consequence of the entire degrees of freedom. This is evident at very high temperature where all the spin degrees of freedom on the three chains contribute, giving an entropy per site that saturates at $k_B\ln 2$. For $\alpha>\alpha_{th}$ (here for $\alpha=10$), the freezing of the spin degrees of freedom manifests itself as a tendency to form a plateau in $S(T)$ at intermediate temperatures.

2. Specific heat

The specific heat is calculated numerically using the relation

$$C=T\frac{dS}{dT}. \quad (21)$$

Figures 15(a) and 15(b) show $C(T)$ as a function of T for several values of α. In panel (a), in comparison to $\alpha=0$, the major effects in the case of $0<\alpha<\alpha_{tr}$ are the reduction of the slope of $C(T)$ at zero T, and the shifting upward of the temperature at which the maximum of $C(T)$ occurs. Near zero T, $C(T)$ is linear in T for all values of α, with the slope about one-third of what it is for the Heisenberg chain.[24] In panel (b), once again one sees the effect of the freezing phenomenon in the splitting of the maximum of $C(T)$ into two maxima for $\alpha>\alpha_{tr}$. While the lower-temperature maximum has the same origin as the maximum of $C(T)$ in the single Heisenberg chain,[24] the higher-temperature maximum is due

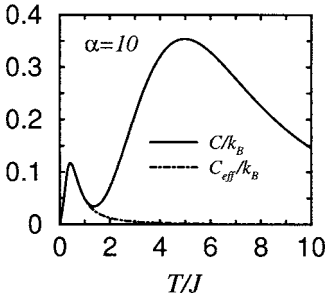

FIG. 16. The specific heat for $\alpha=10$ is compared to the contribution from the lower-energy band $E_1(k)$. The maximum at the higher temperature of $C(T)$ is a consequence of the bands E_2 and E_3.

to the contribution from the bands E_2 and E_3. Note that no sharp peak exists in $C(T)$ because $Q-Q'$ does not vanish at a critical temperature (see Fig. 4).

Figure 16 shows the comparison of $C(T)$ for $\alpha=10$ with the contribution from the band $E_1(k)$, $C_{eff}=TdS_{eff}/dT$, alone. We find that for temperatures smaller than about $1.5J$, $C(T)$ is practically equal to the contribution from this band. As temperature increases $C(T)$ departs from it because the contributions from the bands E_2 and E_3 become important. This finding is consistent with the one found previously for the magnetic susceptibility, and is due to the phenomenon of freezing of part of the spin degrees of freedom.

3. Wilson-Sommerfeld ratio

The ratio of the magnetic susceptibility $\chi(T)$ and the specific heat coefficient $\gamma(T)=C(T)/T$ is a dimensionless quantity, and for $S=1/2$ systems it is defined as[25]

$$R_W=\frac{4\pi^2\chi(T)T}{3C(T)}, \tag{22}$$

and is called the Wilson-Sommerfeld (WS) ratio. For the noninteracting Fermi gas, $R_W=1$ independently of temperature. Both $\chi(T)$ and $\gamma(T)$ are proportional to the density of states (here, at the Fermi energy of the JW fermions, which is zero). The value of unity for R_W reflects on the fact that the electrons in a gas do not interact. The JW fermions in the case of the Heisenberg model form a system of interacting spinless fermions. One therefore expects R_W to deviate from 1 for these interacting JW fermions. Wilson showed that for the Kondo model the impurity contributions to $\chi(0)$ and γ yield $R_W=2$, which does not depend on the strength of the interactions.[26]

Here, Fig. 17(a) shows R_W as a function of temperature for several values of α with $0\leqslant\alpha\leqslant1$. For $T\to0$, R_W approaches 2, and for $T>0.4J$, the T dependence of R_W is consistent with a T^2 dependence. For $\alpha=0$, our result is in good agreement with the results of Johnston and co-workers,[25] who found R_W to be exactly 2 at $T=0$, and a T^2 law at high temperatures. Note however that near zero T, there exists logarithmic contributions which lead to (about 10%) deviations from the value 2. The present approach does not account for these logarithmic contributions to susceptibility and specific heat. What is most important here is that our results are consistent with the trends found in Ref. 25, namely, that with increasing temperature R_W is nearly independent of T up to $T\approx0.4J$.

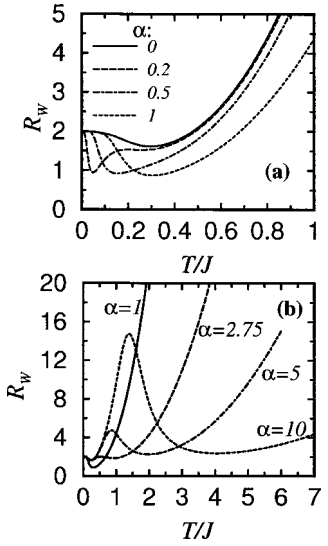

FIG. 17. The WS ratio R_W is plotted as a function of T for various values of the rung-to-leg couplings ratio α.

From the plots of R_W shown in Fig. 17(a) for $\alpha<1$, one sees a significant dependence on α, but the curves show roughly the same functional dependence on temperature as for the single chain. As $T\to0$ the various plots approach 2. For the single chain the minimum value assumed by R_W is ≈1.62, and occurs at $T=0.29J$. For the isotropic ladder with $\alpha=1$, the minimum value of R_W is ≈0.88, and occurs at $T=0.29J$ too. Figure 17(b) shows R_W for values of α larger than 1. For $\alpha<\alpha_{tr}$, the functional dependence on T is more or less similar to that of R_W in the case of $\alpha<1$. However, for $\alpha>\alpha_{tr}$, the T dependence of R_W changes drastically. A maximum appears at an intermediate temperature, and for low temperatures, R_W behaves as for a single chain with the effective coupling J_{eff}; i.e., $R_W\approx R_W^{eff}=4\pi^2\chi_{eff}(T)T/3C_{eff}(T)$. Figure 18 illustrates this for $\alpha=10$. For T smaller than J, R_W and R_W^{eff} are practically the same. The maximum in R_W separates roughly the low-T 1D regime from the higher-T regime where all bands contribute.

IV. CONCLUSIONS

Using the two-dimensional generalized Jordan-Wigner transformation and the bond-mean-field theory, we studied

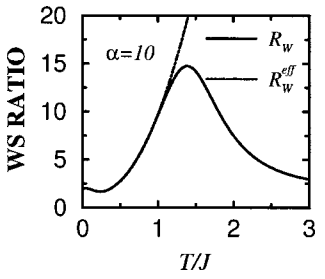

FIG. 18. The ratio R_W is compared to the ratio R_W^{eff} of the Heisenberg chain with the effective coupling J_{eff}.

the Heisenberg model on the three-leg ladder geometry. We found that loose bonds develop in the inner chain and stronger ones in the outer chains. The main results of this work are the proposals of the phenomena of locking and freezing of part of the spin degrees of freedom. For the rung-to-leg couplings ratio α smaller than the threshold value $\alpha_{th}=2.75$, about $2/3$ of the spin degrees of freedom lock into loose singlets at temperatures close to zero. For α greater than the threshold value, these singlets form a coherent state along the chains, causing the three-leg ladder to become equivalent to a single Heisenberg chain with an effective coupling at low enough temperatures. As temperature increases, a crossover to a regime where all the spin degrees of freedom participate takes place. Using the present theory, we obtained a good fit for the susceptibility experimental data for the material $Sr_2Cu_3O_5$. We also calculated the temperature and coupling dependence of the susceptibility, entropy, and specific heat. For coupling α greater than the threshold value, we found that the susceptibility and specific heat present two maxima each. The lower-temperature maximum is of the same origin as in a single Heisenberg chain. The higher-temperature maximum is due to higher-energy excitations that do not exist in a single chain.

ACKNOWLEDGMENTS

The authors thank G. Y. Chitov for his comments on the manuscript. This work was supported by the Laurentian University Research Fund (LURF) and the Natural Science and Engineering Research Council of Canada (NSERC).

*Electronic address: mazzouz@laurentian.ca

[1] T. Barnes, E. Dagotto, J. Riera, and E. S. Swanson, Phys. Rev. B **47**, 3196 (1993).
[2] E. Dagotto and T. M. Rice, Science **271**, 618 (1996).
[3] T. M. Rice, Z. Phys. B: Condens. Matter **103**, 165 (1997).
[4] M. Azzouz, L. Chen, and S. Moukouri, Phys. Rev. B **50**, 6233 (1994).
[5] T. M. Rice, S. Gopalan, and M. Sigrist, Europhys. Lett. **23**, 445 (1993).
[6] D. C. Johnston, M. Troyer, S. Miyahara, D. Lidsky, K. Ueda, M. Azuma, Z. Hiroi, M. Takano, M. Isobe, Y. Ueda, M. A. Korotin, V. I. Asimov, A. V. Mahajan, and L. L. Miller, cond-mat/0001147 (unpublished).
[7] B. Frischmuth, B. Ammon, and M. Troyer, Phys. Rev. B **54**, R3714 (1996).
[8] K. Tandon, S. Lal, S. K. Pati, S. Ramasesha, and D. Sen, Phys. Rev. B **59**, 396 (1999).
[9] D. C. Cabra, A. Honecker, and P. Pujol, Phys. Rev. Lett. **79**, 5126 (1997).
[10] M. Azzouz, Phys. Rev. B **48**, 6136 (1993).
[11] P. Jordan and E. Wigner, Z. Phys. **47**, 631 (1928).
[12] S. R. White, R. M. Noack, and D. J. Scalapino, Phys. Rev. Lett. **73**, 886 (1994).
[13] M. Azuma, Z. Hiroi, M. Takano, K. Ishida, and Y. Kitaoka, Phys. Rev. Lett. **73**, 3463 (1994).
[14] B. Bock and M. Azzouz, Phys. Rev. B **64**, 054410 (2001), and references therein.
[15] I. Affleck and J. B. Marston, Phys. Rev. B **37**, R3774 (1988).
[16] N. D. Mermin and H. Wagner, Phys. Rev. Lett. **17**, 1133 (1966).
[17] M. Azzouz and C. Bourbonnais, Phys. Rev. B **53**, 5090 (1996).
[18] M. Azzouz, B. Dumoulin, and A. Benyoussef, Phys. Rev. B **55**, R11957 (1997).
[19] J. R. Schrieffer, *Theory of Superconductivity* (W. A. Benjamin, New York, 1964).
[20] J. des Cloizeaux and J. J. Pearson, Phys. Rev. **128**, 2131 (1962).
[21] M. Reigrotzki, H. Tsunetsugu, and T. M. Rice, J. Phys.: Condens. Matter **6**, 9235 (1994).
[22] V. N. Muthukumar, C. Gros, R. Valentí, M. Weiden, C. Geibel, F. Steglich, P. Lemmens, M. Fischer, and G. Güntherodt, Phys. Rev. B **55**, 5944 (1997).
[23] M. Azuma (private communication).
[24] J. C. Bonner and M. E. Fisher, Phys. Rev. **135**, A640 (1964).
[25] D. C. Johnston, R. K. Kremer, M. Troyer, X. Wang, A. Klümper, S. L. Bud'ko, A. F. Panchula, and P. C. Canfield, Phys. Rev. B **61**, 9558 (2000).
[26] K. G. Wilson, Rev. Mod. Phys. **47**, 773 (1975).